

**Model Selection using Baryon Acoustic Oscillations  
in the Final SDSS-IV Release**F. Melia<sup>1</sup> and M. López-Corredoira<sup>2,3</sup><sup>1</sup> *Department of Physics, The Applied Math Program, and Department of Astronomy, The University of Arizona, AZ 85721, USA;*<sup>2</sup> *Instituto de Astrofísica de Canarias, E-38205 La Laguna, Tenerife, Spain*<sup>3</sup> *Departamento de Astrofísica, Universidad de La Laguna, E-38206 La Laguna, Tenerife, Spain*

Received 15 February 2022

Revised 29 March 2022

Communicated by Managing Editor

The baryon acoustic oscillation (BAO) peak, seen in the cosmic matter distribution at redshifts up to  $\sim 3.5$ , reflects the continued expansion of the sonic horizon first identified in temperature anisotropies of the cosmic microwave background. The BAO peak position can now be measured to better than  $\sim 1\%$  accuracy using galaxies, and  $\sim 1.4 - 1.6\%$  precision with Ly- $\alpha$  forests and the clustering of quasars. In conjunction with the Alcock-Paczyński (AP) effect, which arises from the changing ratio of angular to spatial/redshift size of (presumed) spherically-symmetric source distributions with distance, the BAO measurement is viewed as one of the most powerful tools to use in assessing the geometry of the Universe. In this paper, we employ five BAO peak measurements from the final release of the Sloan Digital Sky Survey IV, at average redshifts  $\langle z \rangle = 0.38, 0.51, 0.70, 1.48$  and  $2.33$ , to carry out a direct head-to-head comparison of the standard model,  $\Lambda$ CDM, and one of its principal competitors, known as the  $R_h = ct$  universe. For completeness, we complement the AP diagnostic with a volume-averaged distance probe that assumes a constant comoving distance scale  $r_d$ . Both probes are free of uncertain parameters, such as the Hubble constant, and are therefore ideally suited for this kind of model selection. We find that  $R_h = ct$  is favored by these measurements over the standard model based solely on the AP effect, with a likelihood  $\sim 75\%$  versus  $\sim 25\%$ , while *Planck*- $\Lambda$ CDM is favored over  $R_h = ct$  based solely on the volume-averaged distance probe, with a likelihood  $\sim 80\%$  versus  $\sim 20\%$ . A joint analysis using both probes produces an inconclusive outcome, yielding comparable likelihoods to both models. We are therefore not able to confirm with this work that the BAO data, on their own, support an accelerating Universe.

*Keywords:* cosmology: cosmological parameters – cosmology: distance scale – cosmology: observations – quasars: general

**1. Introduction**

The early Universe contained photons, leptons and baryons coupled tightly via Compton scattering processes and Coulomb interactions. The tussle between gravity and radiation pressure generated oscillations and waves around overdense regions

that propagated outwards, dragging baryons and leptons along with them. Eventually, the Universe cooled sufficiently for neutral atoms to form, after which the radiation detached from the matter, leaving a fossilized imprint of the waves with a characteristic *comoving* scale which, in the standard model ( $\Lambda$ CDM), is estimated to be  $r_d \sim 147$  Mpc.

This acoustic feature set the  $(0.596724 \pm 0.00038)^\circ$  scale for the peaks seen in the angular power spectrum of the cosmic microwave background (CMB)<sup>1</sup>, and continued to grow with the expansion of the Universe to influence late time galaxy formation and evolution<sup>2,3,4,5</sup>. Its presence is now seen in both Fourier and configuration space<sup>6,7</sup>. In this picture, the baryon acoustic oscillations (BAO), as these frozen imprints are known, retained a constant comoving size after recombination, but stretched to galaxy-cluster size along with the overall Hubble expansion. The BAO thus represent a ‘standard ruler’ in comoving space that one may use with measurements at different redshifts to trace the expansion history of the Universe.

**Table 1.** Final SDSS-IV BAO Peak Data and the measured values of  $y(z)$ . With the exception of the datum at  $\langle z \rangle = 2.33$ , all the measurements correspond to the consensus constraints from the combination of Fourier and configuration space BAO analyses, with the inclusion of a systematic error budget.

$\langle z \rangle$	$d_A/r_d$	$d_H/r_d$	$C(d_A, d_H)$	$y(z)$	Reference
0.38	$7.41 \pm 0.12$	$25.00 \pm 0.76$	-0.29	$1.076 \pm 0.041$	13,17
0.51	$8.85 \pm 0.14$	$22.33 \pm 0.58$	-0.50	$1.173 \pm 0.043$	13
0.70	$10.51 \pm 0.19$	$19.33 \pm 0.53$	-0.50	$1.320 \pm 0.052$	18,19
1.48	$12.38 \pm 0.32$	$13.26 \pm 0.55$	-0.50	$1.564 \pm 0.092$	11,12
2.33	$11.26 \pm 0.33$	$8.99 \pm 0.19$	-0.40	$1.790 \pm 0.076$	16

Over the past two decades, the Sloan Digital Sky Survey (SDSS)<sup>8</sup> has constructed several diverse spectroscopic catalogs of galaxies and quasars one may use to map the large-scale structure of the Universe. The last of these programs, called eBOSS (extended Baryon Oscillation Spectroscopic Survey)<sup>9</sup>, in the fourth phase of SDSS (referred to as SDSS-IV)<sup>10</sup>, includes four main tracers: luminous red galaxies, emission-line galaxies, quasars, and a separate high-redshift quasar sample for the study of the Ly- $\alpha$  forest. The eBOSS program came to an end on March 1st, 2019.

In this paper, we shall adopt source bins from three of these catalogs with effective (i.e., ‘average’) redshifts ranging from 0.38 to 2.33. The BAO detection using quasars as tracers<sup>11,12</sup> at  $0.8 \lesssim z \lesssim 2.2$  bridges the gap between the lower redshift SDSS galaxy surveys<sup>13,14</sup> at  $z \lesssim 0.8$  and the Ly- $\alpha$  forest<sup>15,16</sup> at  $z \gtrsim 2.2$ .

A principal motivation for the analysis we carry out here, based on the use

of these BAO measurements with the Alcock-Paczyński effect described below<sup>20</sup>, complemented by a volume-averaged distance probe that assumes a constant value of  $r_d$ , is the significant improvement achieved recently in mitigating the contamination due to so-called redshift-space distortions. These are due to peculiar velocities induced by gravitational influences within the clusters themselves<sup>21,22,23</sup>, but methods have been developed to break the degeneracy based on the notion that the distortions affect primarily the amplitude of the BAO peak, while their impact on its position is negligible<sup>24</sup>. And it is the BAO peak's position that determines the standard ruler used for the Alcock-Paczyński and volume-averaged distance tests.

This outcome is achieved via reconstruction techniques<sup>25,26</sup> that enhance the quality of the galaxy two-point correlation function. In addition, the newer Ly- $\alpha$  and quasar auto- and cross-correlation functions may not be as precise as the BAO peak position measured with galaxies (i.e.,  $\sim 1\%$ ), but are still sufficiently accurate to provide a BAO peak position with an accuracy better than  $\sim 1.4\%$  and  $\sim 1.6\%$ , respectively<sup>27</sup>. One should note that all of these measurements use a template for the correlation function drawn from the concordance model, which could create a problem when one uses alternative cosmologies. But the actual shape of the BAO peak barely influences the determination of its centroid position, both parallel to the line-of-sight and in the perpendicular direction, as long as its FWHM is very narrow. For the most recent measurements we use in this analysis, the overall redshift distortions produce systematic errors of order  $\lesssim 0.5\%$  in the angular-diameter ( $d_A[z]$ ) and comoving ( $d_{\text{com}}[z]$ ) distances—an impressive feat, given that statistical errors as small as  $\sim 4\%$  are now achievable (see refs. <sup>12,14</sup>; see also refs. <sup>18,11,19</sup>).

In the next section, we describe how the BAO peak positions can be used to assess the geometry of the Universe in a model-independent way, even without knowing a precise value for the Hubble constant,  $H_0$ . Our use of this approach in an earlier application based on older data<sup>28</sup> produced a very intriguing outcome, notably that the model preferred by the BAO data is not necessarily  $\Lambda$ CDM. A principal goal of such studies is to probe the hypothesized late-time acceleration of the Universe's expansion. In this paper, we carry out this analysis using the updated, final SDSS-IV release to test three competing cosmologies: (i) *Planck*- $\Lambda$ CDM<sup>1</sup>; (ii)  $\Lambda$ CDM with its matter-density ( $\Omega_m$ ) as a free, optimizable parameter, and (iii) the  $R_h = ct$  universe<sup>29,30</sup>, whose viability has been established previously using over 27 different kinds of data. The critical difference between a cosmology based on  $\Lambda$ CDM versus one characterized by  $R_h = ct$  is that, while the former accelerates, the latter always expands at a constant rate.

## 2. BAO Probes

### 2.1. The Alcock-Paczyński Test

The measurements of  $d_A(z)/r_d$  and  $d_{\text{com}}(z)/r_d$  described above are ideally suited to the Alcock-Paczyński<sup>20</sup> test we shall now describe. Critically, the actual value

of  $r_d$  is not required, nor is the Hubble constant,  $H_0$ , whose measurements at low and high redshifts now appear to be inconsistent with each other at a  $4.4\sigma$  level of significance. The Hubble constant characterizes the current expansion rate of the Universe and determines its *absolute* distance scale, but as the accuracy with which it is measured continues to improve, its value<sup>1</sup> ( $67.4 \pm 0.5 \text{ km s}^{-1} \text{ Mpc}^{-1}$ ) inferred from the CMB in the context of flat  $\Lambda$ CDM contrasts with that ( $74.03 \pm 1.42 \text{ km s}^{-1} \text{ Mpc}^{-1}$ ) based on local Type Ia supernovae calibrated with the Cepheid distance ladder<sup>31</sup>. A cosmological probe that avoids having to use  $H_0$ —such as the Alcock-Paczyński test we employ here—therefore has a significant advantage over others that require the measurement of absolute distances.

Assuming we have a spherically-symmetric distribution of objects (or, equivalently, a standard ruler whose length in the comoving frame is independent of orientation with respect to our line-of-sight), with radius

$$\begin{aligned} L_{\parallel} &= \Delta z \frac{d}{dz} d_{\text{com}}(z) \\ &= \Delta z d_{\text{H}}(z) \end{aligned} \quad (1)$$

along the line-of-sight and

$$L_{\perp} = \Delta\theta(1+z)d_{\text{A}}(z) \quad (2)$$

in the perpendicular direction, the ratio

$$y(z) \equiv \frac{\Delta z}{z\Delta\theta} \frac{L_{\perp}}{L_{\parallel}} \quad (3)$$

depends only on the cosmological comoving distance,  $d_{\text{com}}(z)$ , and the angular-diameter distance,  $d_{\text{A}}(z)$  and, very importantly, is independent of any source evolution. The quantity  $d_{\text{H}}(z)$  is the Hubble distance defined in Equation (7) below.

These two distances are simply related according to the equation<sup>29,30</sup>

$$d_{\text{com}}^R(z) = (1+z)d_{\text{A}}^R(z) = \frac{c}{H_0} \ln(1+z), \quad (4)$$

in the case of  $R_{\text{h}} = ct$  and, more generally, via the parametrized formulation

$$d_{\text{com}}^{\Lambda}(z) = (1+z)d_{\text{A}}^{\Lambda}(z) = \frac{c}{H_0} \int_0^z \frac{du}{\sqrt{\Omega_{\text{m}}(1+u)^3 + \Omega_{\Lambda}}}, \quad (5)$$

in  $\Lambda$ CDM. This expression assumes spatial flatness and ignores the infinitesimal contribution from radiation in the redshift range of interest. It also employs the conventional definition of a scaled density,  $\Omega_i$ , representing the energy density of species  $i$  normalized to today's critical density,  $\rho_c \equiv 3c^2 H_0^2 / 8\pi G$ .

It is therefore rather trivial to see that

$$y(z) = \frac{(1+z)}{z} \frac{d_{\text{A}}(z)}{d_{\text{H}}(z)}, \quad (6)$$

where

$$d_{\text{H}} \equiv \frac{c}{H(z)}, \quad (7)$$

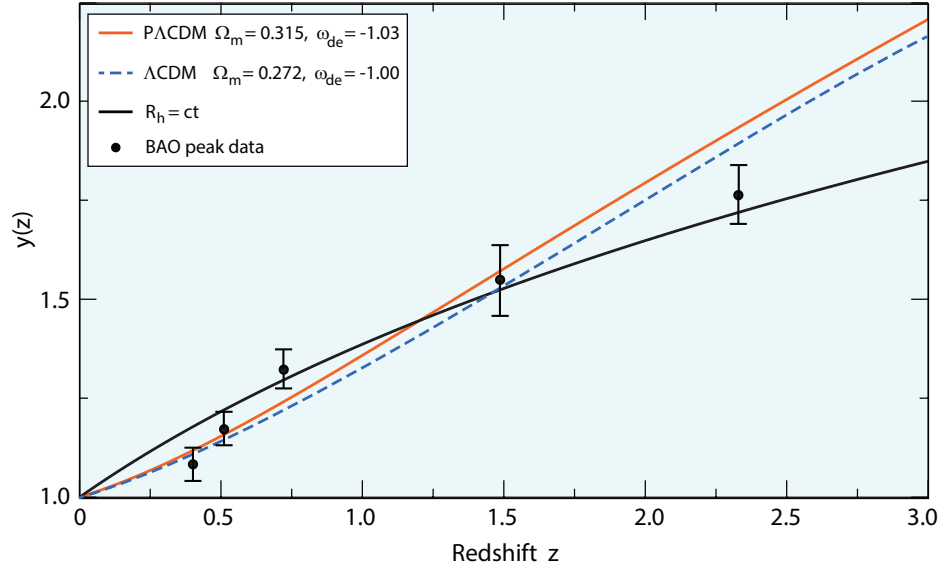


Fig. 1. Ratio of observed angular size to radial/redshift size,  $y(z)$ , versus redshift,  $z$ , inferred from five BAO peak measurements at  $\langle z \rangle = 0.38, 0.51, 0.70, 1.48$  and  $2.33$ . Note, however, that the three lowest-redshift data points are not completely independent (see text). The data are compared to the predictions of 3 models: (i) (red solid) *Planck*- $\Lambda$ CDM, with (pre-optimized) parameters  $\Omega_m = 0.315$  and  $w_{de} = -1.03$ , (ii) (blue dash) a best-fit  $\Lambda$ CDM cosmology using  $\Omega_m$  as a free parameter (with optimized value  $0.292 \pm 0.038$ , and a fixed  $w_{de} = -1.00$ ), and (iii) (black solid) the  $R_h = ct$  universe, whose  $y(z)$  function is completely free of any parameters.

and

$$H^R(z) \equiv H_0(1+z), \quad (8)$$

for  $R_h = ct$ , while

$$H^\Lambda(z) \equiv H_0 \sqrt{\Omega_m(1+z)^3 + \Omega_\Lambda}, \quad (9)$$

for the standard model. Clearly, both  $H_0$  and  $r_d$  cancel completely in  $y(z)$  when we write

$$y(z) = \frac{(1+z)}{z} \frac{d_A(z)/r_d}{d_H(z)/r_d}, \quad (10)$$

allowing us to utilize the data in Table 1 in a model-independent fashion. This compilation includes five measurements of  $d_A/r_d$  and  $d_H/r_d$ , their individual errors, and the correlation coefficient between  $d_A$  and  $d_H$ , labeled  $C(d_A, d_H)$ , in column 4. The uncertainty in  $y(z)$  is estimated according to the error propagation equation

$$\sigma_y^2 = \left( y \frac{\sigma_{d_A}}{d_A} \right)^2 + \left( y \frac{\sigma_{d_H}}{d_H} \right)^2 - 2y^2 \frac{\sigma_{d_A, d_H}}{d_A d_H}, \quad (11)$$

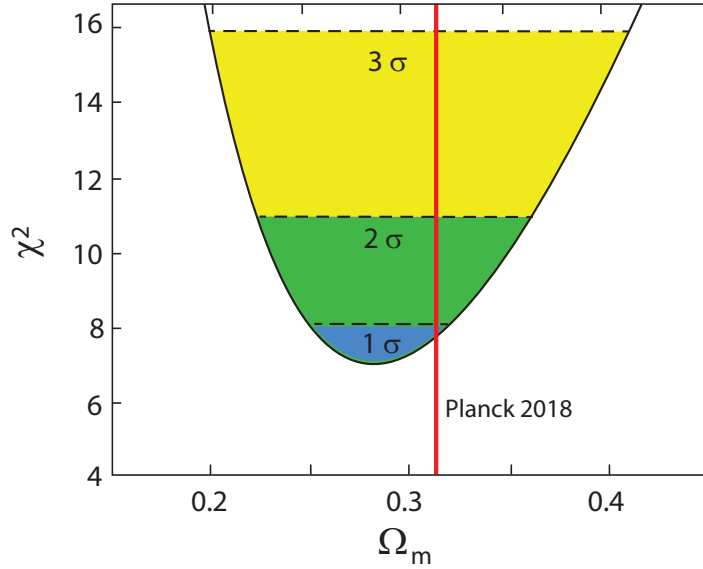


Fig. 2. Optimization of the matter density parameter  $\Omega_m$  for the  $\Lambda$ CDM model in figure 1, with the  $1\sigma = 0.04$ ,  $2\sigma$  and  $3\sigma$  confidence levels in a Gaussian distribution, i.e., 68.3% (cyan), 95.4% (green) and 99.73% (yellow). By comparison, the *Planck*- $\Lambda$ CDM (concordance) model corresponds to the optimized parameter value  $\Omega_m = 0.315 \pm 0.007$ , which is consistent with our best fit value ( $\Omega_m = 0.272 \pm 0.041$ ) to within  $1\sigma$ .

where

$$\sigma_{d_A, d_H} \equiv C(d_A, d_H) \sigma_{d_A} \sigma_{d_H} . \quad (12)$$

Figure 1 shows the function  $y(z)$  measured with the five BAO data points summarized in Table 1, along with the predictions of three models: (i) (solid black)  $R_h = ct$ ; (ii) (solid red) *Planck*- $\Lambda$ CDM (with pre-optimized parameters  $\Omega_m = 0.315$ ,  $\Omega_{de} = 1 - \Omega_m$ , and a dark-energy equation-of-state parameter<sup>1</sup>  $w_{de} = -1.003$ ); and (iii) (dashed blue) a more generic  $\Lambda$ CDM model with a free  $\Omega_m$  variable. In this case, the fit is optimized with a matter density  $\Omega_m = 0.272 \pm 0.041$  (see also fig. 2), which is consistent to within  $1\sigma$  with the *Planck* value.

The quality of each fit may be assessed via its corresponding reduced  $\chi^2$  value, i.e.,  $\chi_{\text{dof}}^2 \equiv \chi^2/[N - \nu]$ , where  $N$  is the number of independent data points and  $\nu$  is the number of free parameters in the model. The bins used to obtain the two lowest-redshift measurements in this set overlap somewhat and are therefore not completely independent. They provide a net redshift coverage of 0.4, but their bins span a total range of 0.5. We therefore estimate the ‘effective’ number of independent points as  $2 \times (0.4/0.5) = 1.6$  for this subset, yielding a total number  $N = 4.6$  of

independent data points. In estimating the  $\chi^2$  for each model, we thus use

$$\chi^2 = \sum_{i=1}^5 f_i \frac{[y_{\text{th}}(z_i) - y(z_i)]^2}{\sigma_{y(z_i)}^2}, \quad (13)$$

where  $y_{\text{th}}$  is the theoretical value,  $y(z_i)$  is the observed quantity, and  $f_i = 0.8$  for  $i = 1-2$ , and  $f_i = 1$  for points 3 to 5.

**Table 2.** Model comparison using the effective number,  $N = 4.6$ , of BAO peak data points, based on (i) the reduced  $\chi_{\text{dof}}^2 \equiv \chi^2/(N - \nu)$ , with  $\nu =$  number of free parameters; (ii) optimized parameters (if any); (iii) AIC; and (iv) KIC (see § 3).

Model	$\chi_{\text{dof}}^2$	Parameter	AIC	KIC
$\Lambda$ CDM	1.84	$\Omega_{\text{m}} = 0.272 \pm 0.041$	8.61	9.61
<i>Planck</i> - $\Lambda$ CDM	1.74	–	8.00	8.00
$R_{\text{h}} = ct$	1.43	–	6.58	6.58

In the Appendix, we gauge the impact of this approach using a covariance matrix available online<sup>a</sup> for  $d_{\text{com}}$  and  $d_{\text{H}}$  in the binnings at  $z = 0.38$  and  $0.51$ , along with an estimate of the number of galaxies in the overlapping redshift regions based on the overlap redshift intervals. A comparison of the results summarized in Tables 5 and 6 with those shown in Tables 2 and 4 suggests that these two procedures, using Equations (13) and (21), produce only minor relative changes to the outcome of our model comparison. The model prioritization, however, remains unchanged.

Very interestingly, this Alcock-Paczyński test, based on BAO measurements, provides an optimized matter density parameter,  $\Omega_{\text{m}} = 0.272 \pm 0.041$  (or  $0.276 \pm 0.041$  if we instead use Eq. 21), fully consistent (to within  $1\sigma$ ) with its *Planck* value. One can see this quite easily by comparing the two curves in Figure 1, which show that the optimized fit to  $y(z)$  is very close to that of the *Planck*- $\Lambda$ CDM prediction (see also Fig. 2). Quite tellingly, however, this figure also demonstrates why  $R_{\text{h}} = ct$  is favored by the BAO data and the AP diagnostic over both *Planck*- $\Lambda$ CDM and the more generic version of  $\Lambda$ CDM with a variable  $\Omega_{\text{m}}$  (see Table 2). It should also be stressed that  $R_{\text{h}} = ct$  has no free parameters at all for this comparison with the data. In other words, these cosmologies are not all nested, so a statistically fair comparison needs to take into account the different numbers of free parameters. We shall address this issue in § 3 below.

<sup>a</sup><https://svn.sdss.org/public/data/eboss/DR16cosmo/tags/v1-0-1/likelihoods/BAO-only/>

## 2.2. Volume-averaged distance probe

The AP effect offers a clean cosmological test that requires minimal assumptions, but it ignores another possibly important piece of information, i.e., that the comoving scale  $r_d$  characterizing the BAO signal should be the same at all redshifts—at least in the context of  $\Lambda$ CDM. The volume-averaged distance probe is thus not as clean as the AP effect, which is based solely on the geometry, whereas the former must make some assumption concerning the evolution (or not) of the comoving scale  $r_d$ . Nevertheless, we shall here assume for simplicity that  $r_d$  is indeed constant in the models we examine.

**Table 3.** Final SDSS-IV BAO Peak Data and the measured values of  $x(z)$ .

$\langle z \rangle$	$d_A/r_d$	$d_H/r_d$	$C(d_A, d_H)$	$x(z)$	Reference
0.38	$7.41 \pm 0.12$	$25.00 \pm 0.76$	-0.29	$1.000 \pm 0.022$	13,17
0.51	$8.85 \pm 0.14$	$22.33 \pm 0.58$	-0.50	$1.269 \pm 0.042$	13
0.70	$10.51 \pm 0.19$	$19.33 \pm 0.53$	-0.50	$1.632 \pm 0.084$	18,19
1.48	$12.38 \pm 0.32$	$13.26 \pm 0.55$	-0.50	$2.650 \pm 0.120$	11,12
2.33	$11.26 \pm 0.33$	$8.99 \pm 0.19$	-0.40	$3.095 \pm 0.116$	16

A complete analysis of BAO measurements often includes a constraint on the ratio  $D_v(z)/r_d$ , where the volume-averaged distance  $D_v(z)$  is defined as

$$\begin{aligned}
 D_v(z) &\equiv \{z d_{\text{com}}(z)^2 d_H(z)\}^{1/3} \\
 &= \{z(1+z)^2 d_A(z)^2 d_H(z)\}^{1/3} .
 \end{aligned}
 \tag{14}$$

Together, the AP and  $D_v$  diagnostics constitute a more complete representation of the full information content of the BAO signal—assuming, of course, that  $r_d$  is indeed constant in all the models being tested. Using the volume-averaged distance  $D_v$  on its own, however, would require a model-dependent prediction of  $r_d$ , which would complicate the analysis, and possibly weaken the model comparison. Instead, we shall use the ratio

$$x(z) \equiv \frac{D_v(z)/r_d}{D_v(z_p)/r_d} ,
 \tag{15}$$

using a ‘pivot’ redshift,  $z_p$ , for each of the remaining four measurements. We choose the pivot point  $\langle z \rangle = 0.38$ . In the case of  $y(z)$ , the values of  $r_d$  and  $H_0$  completely cancel out. The volume-averaged distance probe,  $x(z)$ , is also independent of both  $r_d$  and  $H_0$ , though the required use of the ratio in Equation (15) then leaves us with only four data points, which are shown in Table 3. The uncertainty in  $x(z)$  is



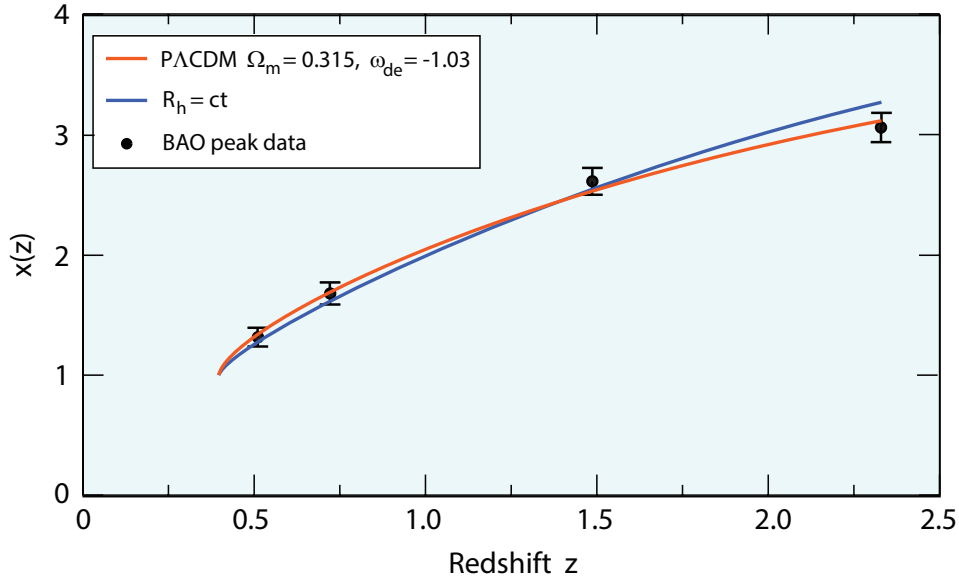


Fig. 3. The volume-averaged quantity  $x(z)$  (see Eq. 15), versus redshift,  $z$ , inferred from the four BAO peak measurements at  $\langle z \rangle = 0.51, 0.70, 1.48$  and  $2.33$  (see Table 3). The datum at  $\langle z \rangle = 0.38$  is not included because it is used as the ‘pivot’ point (see Eq. 15 and Table 3). The data are compared to the predictions of 2 models: (i) (red solid) *Planck*- $\Lambda$ CDM, with (pre-optimized) parameters  $\Omega_m = 0.315$  and  $w_{de} = -1.03$ , and (ii) (blue solid) the  $R_h = ct$  universe, whose  $x(z)$  function is completely free of any parameters.

estimated according to the error propagation equation

$$\sigma_x^2 = \left( x \frac{2\sigma_{d_A}}{3d_A} \right)^2 + \left( x \frac{\sigma_{d_H}}{3d_H} \right)^2 - 2x^2 \frac{\sigma_{d_A \cdot d_H}}{d_A d_H} + \left( x \frac{\sigma_{\text{piv}}}{x(0.38)} \right)^2, \quad (16)$$

where

$$\sigma_{d_A \cdot d_H} \equiv C(d_A, d_H) \sigma_{d_A} \sigma_{d_H}, \quad (17)$$

and  $\sigma_{\text{piv}}$  is the error in the pivot value  $x(0.38)$ . (Note that the last term in Eq. 16 is used only for the non-pivot points.)

The volume-averaged quantity  $x(z)$  is shown in figure 3 for the four measured BAO data points summarized in Table 3, along with the predictions of: (i) (solid blue)  $R_h = ct$ , and (ii) (solid red) *Planck*- $\Lambda$ CDM (with pre-optimized parameters  $\Omega_m = 0.315$ ,  $\Omega_{de} = 1 - \Omega_m$ , and a dark-energy equation-of-state parameter<sup>1</sup>  $w_{de} = -1.003$ ). The curve corresponding to the optimization of  $\Lambda$ CDM with one free parameter is very similar to these two curves, so we omit it for the sake of clarity.

In this case, all four of the data points are independent of each other. The  $\chi^2$  values for the three models are 3.216 (yielding  $\chi_{\text{dof}}^2 = 0.804$ ) for  $R_h = ct$ , 0.421 (yielding  $\chi_{\text{dof}}^2 = 0.105$ ) for *Planck*- $\Lambda$ CDM, and 0.409 (yielding  $\chi_{\text{dof}}^2 = 0.105$ ) for  $\Lambda$ CDM, with an optimized matter density parameter  $\Omega_m = 0.308 \pm 0.040$ . Based

solely on their values of  $\chi^2$ , all three models fit the volume-averaged distances very well. As we shall see in § 3, however, the information criteria somewhat favor both *Planck*- $\Lambda$ CDM and  $\Lambda$ CDM over  $R_h = ct$ . We shall quantitatively assess the impact of these measurements on the overall model selection in the next section.

### 3. Model Selection

To compare models with a different number of free parameters, constituting an uneven flexibility in fitting the data, it is now common in cosmology to carry out model selection via the use of information criteria. These include the Akaike Information Criterion<sup>32,33,34,35</sup>,

$$\text{AIC} \equiv \chi^2 + 2\nu, \quad (18)$$

and the Kullback Information Criterion<sup>36</sup>,

$$\text{KIC} \equiv \chi^2 + 3\nu. \quad (19)$$

**Table 4.** Head-to-head model comparisons using the AIC and KIC values in Table 2, and those corresponding to the fits shown in Fig. 3.

Model Comparison	$\Delta\text{AIC}$	AIC	$\Delta\text{KIC}$	KIC
<u>AP effect only</u>				
<i>Planck</i> - $\Lambda$ CDM vs. $R_h = ct$	1.42	33% vs. 67%	1.42	33% vs. 67%
$\Lambda$ CDM vs. $R_h = ct$	2.03	27% vs. 73%	3.03	18% vs. 82%
<u>Volume averaged distance only</u>				
<i>Planck</i> - $\Lambda$ CDM vs. $R_h = ct$	-2.79	80% vs. 20%	-2.79	80% vs. 20%
$\Lambda$ CDM vs. $R_h = ct$	-0.81	60% vs. 40%	0.19	48% vs. 52%
<u>Combined test</u>				
<i>Planck</i> - $\Lambda$ CDM vs. $R_h = ct$	-1.37	66% vs. 34%	-1.37	66% vs. 34%
$\Lambda$ CDM vs. $R_h = ct$	-0.37	55% vs. 45%	1.37	33% vs. 67%

A third variant, known as the Bayes Information Criterion<sup>37</sup>, is an asymptotic ( $N \rightarrow \infty$ ) approximation to the outcome of a conventional Bayesian inference procedure for deciding between models. This criterion, however, is reliable only when the number of data points  $N$  is large (i.e.,  $\gg 20$ ). For the analysis in this paper, we have  $N = 4.8$  using the AP probe, and 4 for the volume-averaged measure of distance,  $x(z)$ , so we restrict our attention solely to the AIC and KIC.

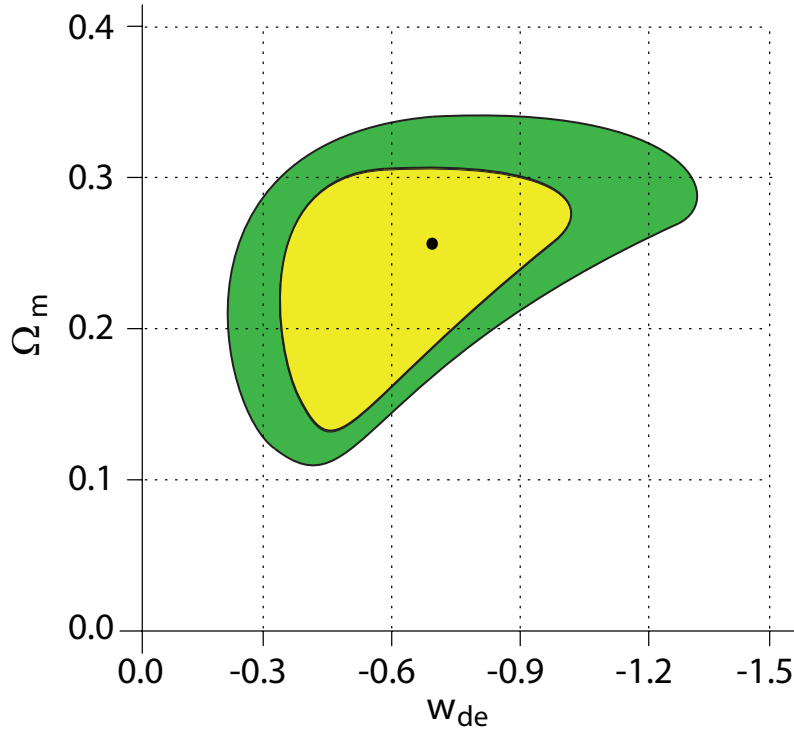


Fig. 4. Confidence level contours as a function of  $\Omega_m$  and  $w_{de}$  for the  $w$ CDM model with two free parameters optimized via the combined AP and volume-averaged distance probes. The two levels are equivalent to  $1-2\sigma$  in a Gaussian distribution (i.e., 68.3% C.L., yellow; 98.4% C.L., green). The best fit parameters, indicated by the black dot, are  $\Omega_m = 0.256 \pm 0.081$  and  $w_{de} = -0.68 \pm 0.31$ . Both differ from the *Planck* optimization adopted for the *Planck*- $\Lambda$ CDM model included in Tables 2 and 4, but are nevertheless consistent with those values to within  $1\sigma$ .

These information criteria provide a consistent way to assess which model is favored by the data. For model  $\mathcal{M}_\alpha$ , the unnormalized confidence of it being ‘true’ is the Akaike weight  $\exp(-AIC_\alpha/2)$ . In a head-to-head comparison between two competing models, its relative likelihood of being the correct choice is therefore

$$P(\mathcal{M}_\alpha) = \frac{\exp(-AIC_\alpha/2)}{\exp(-AIC_1/2) + \exp(-AIC_2/2)}. \quad (20)$$

An analogous expression is used for KIC. In Table 4, we show the model comparison likelihoods for  $y(z)$  only,  $x(z)$  only, and finally for the joint test using *both* the AP and volume-averaged distance probes.

The reduced  $\chi^2_{dof}$  values in Table 2 and the percentage likelihoods in Table 4 show that the application of the Alcock-Paczyński test to the BAO peak data favors the  $R_h = ct$  universe over both *Planck*- $\Lambda$ CDM and flat  $\Lambda$ CDM with an adjustable  $\Omega_m$  parameter. The generic version of  $\Lambda$ CDM optimized to fit these BAO data is fully consistent with the *Planck* model.

When the BAO data are used with the volume-averaged distance probe,  $D_v$ , however, the likelihoods are reversed. Based solely on their  $\chi_{\text{dof}}^2$  values, both  $R_h = ct$  and *Planck*- $\Lambda$ CDM fit the  $x(z)$  data comparably well. The information criteria, however, show a tangible preference for the concordance model over  $R_h = ct$ , with likelihoods  $\sim 80\%$  versus  $\sim 20\%$ . But the outcome based on the volume-averaged distance probe is inconclusive when comparing  $\Lambda$ CDM and  $R_h = ct$ , yielding comparable likelihoods for both models.

The most compelling model selection ought to be the joint analysis using both the AP and volume-averaged distance probes, whose outcome is also summarized in Table 4. As one can see, however, this procedure yields comparable likelihoods for all three models, suggesting that the BAO data used in conjunction with the AP and  $D_v$  tests do not strongly support the idea that the Universe is currently accelerating.

Finally, we address the possibility that restricting  $\Lambda$ CDM to just one free parameter may be inhibiting its ability to fit the BAO data. We have therefore also carried out the joint analysis for model selection between  $R_h = ct$  and  $w$ CDM, in which we relax the requirement that dark energy be a cosmological constant. In this case, the standard model has two free parameters:  $\Omega_m$  and the dark-energy equation of state variable  $w_{\text{de}}$ .

The results of this comparison are summarized in Figure 4, which shows the confidence level contours as a function of  $\Omega_m$  and  $w_{\text{de}}$ . Based on the joint AP- $D_v$  analysis, the  $w$ CDM model best fits the BAO data with the optimized parameters  $\Omega_m = 0.256 \pm 0.081$  and  $w_{\text{de}} = -0.68 \pm 0.31$ . These are noticeably different from their *Planck* counterparts, but are consistent with them to within  $1\text{-}\sigma$ . In this case, the AIC assigns the likelihoods 55% versus 45% favoring  $w$ CDM over  $R_h = ct$ , while the KIC favors  $R_h = ct$  over  $w$ CDM with likelihoods 69% versus 31%. Notice also that the likelihoods for  $w$ CDM are virtually indistinguishable from those assigned to  $\Lambda$ CDM. This happens because the greater flexibility afforded by the extra free parameter in  $w$ CDM is mitigated by the additional penalty assigned to this model by the information criteria. In other words, our joint analysis using both the AP and  $D_v$  probes does not provide a clear indication of which model is favored by the BAO data.

#### 4. Discussion and Conclusion

The analysis we have carried out is based exclusively on the Alcock-Paczyński effect, formalized in Equation (10), and the volume-averaged distance measure, defined in Equation (15). The data corresponding to the BAO scale constitute independent measurements of the comoving distance,  $d_{\text{com}}(z)/r_d$ , and the Hubble distance,  $d_H/r_d = c/H(z)r_d$ , in terms of the sonic radius  $r_d$ .

As we have highlighted throughout this paper, the Alcock-Paczyński diagnostic is unique (and the cleanest) because it is simply proportional to  $(d_{\text{com}}/r_d)/(d_H/r_d)$ . Thus,  $H_0$  and  $r_d$  completely cancel out, so one does not need to deal with these

imprecisely known parameters. Other combinations of these distances depend to some degree on the ratio  $Q \equiv c/H_0 r_d$ , which is unknown. Nevertheless, by defining the quantity  $x(z)$  in Equation (15), one may still avoid using the model-dependent radius  $r_d$ . Unfortunately, this reduces the number of available data points, but the joint analysis using both the AP and  $D_v$  effects has produced some very useful results.

In light of this work, we do not find direct evidence from the BAO peak measurements that the Universe is currently accelerating. The model favored by the AP test on its own is  $R_h = ct$ , which has an expansion factor  $a(t) \propto t$ , suggesting that the cosmic expansion is proceeding at a constant rate. In fact, this model fits the BAO data better than *Planck*- $\Lambda$ CDM and  $\Lambda$ CDM with an optimizable  $\Omega_m$ , and it does this *without* the benefit of any free parameters. In addition, the value of  $H_0$  is not required for any of this analysis, so its uncertain nature cannot be used as a possible reason for this disparity.

Interestingly, however, the model selection is reversed when the volume-averaged distance measure is used on its own. Not surprisingly, one therefore finds that a joint analysis using both the AP and  $D_v$  diagnostics yields inconclusive evidence, favoring neither model over the other.

Nevertheless, it is useful to point out from Figure 1 that the datum most important to this outcome is that corresponding to the Ly- $\alpha$  measurement at  $\langle z \rangle = 2.33$ , which is arguably the most precise of the set we have used. The fact that this measurement is in tension with the standard model has been noted before<sup>38,15</sup>, though the final SDSS-IV eBOSS release has cemented this disparity more emphatically. The prediction of  $y(2.33) = 1.96$  by *Planck*- $\Lambda$ CDM differs from the measured value by over  $2.2\sigma$ . This inconsistency has been reconsidered following each successive enhancement of the SDSS quasar catalog, and is now established rather solidly. It provides an important affirmation of the turnover in  $y(z)$  expected towards higher redshifts in  $R_h = ct$ , which is completely lacking in  $\Lambda$ CDM (see fig. 1).

Our conclusion that the BAO peak measurements in the final SDSS-IV release, together with the Alcock-Paczyński and  $D_v$  tests, do not favor either the  $R_h = ct$  universe or  $\Lambda$ CDM- $w$ CDM, suggests that the BAO observations, on their own, cannot be used to argue for an accelerating Universe. This conclusion somewhat confirms the outcome of many other comparative tests based on a broad range of observations. A recent compilation of these results may be found in Table 2 of ref. <sup>39</sup>. The impact of the work reported in this paper is being explored elsewhere, particularly with regard to the growing likelihood that inflation may not have worked as expected, and may in fact have never happened<sup>40,41</sup>.

## Acknowledgments

We are very grateful to the anonymous referee for their thoughtful and helpful review, which has led to several notable improvements to the contents of this manuscript. F.M. is also grateful to Amherst College for its support through a

John Woodruff Simpson Lectureship. MLC acknowledges support from the Spanish Ministry of Economy and Competitiveness (MINECO) under the grant PGC-2018-102249-B-100.

## References

1. Planck Collaboration, *A&A* **641** (2020) A6.
2. P.J.E. Peebles & J. T. Yu, *Astrophys. J.* **162** (1970) 815.
3. R. A. Sunyaev & Ya. B. Zeldovich, *Astrophys. & Sp. Sc.* **7** (1970) 3.
4. J. R. Bond & G. Efstathiou, *Mon. Not. R. Astron. Soc.* **226** (1987) 655.
5. W. Hu & M. White, *Astrophys. J.* **471** (1996) 30.
6. S. Cole, *Mon. Not. R. Astron. Soc.* **362** (2005) 505.
7. D. J. Eisenstein et al., *Astrophys. J.* **633** (2005) 560.
8. D. G. York, J. Adelman, J. E. Jr, Anderson, F. Scott, J. Annis, N. A. Bahcall et al., *AJ* **120** (2000) 1579.
9. K. S. Dawson, J.-P. Kneib, W. J. Percival, S. Alam, F. D. Albareti, S. F. Anderson et al., *AJ* **151** (2016) 44.
10. M. R. Blanton, M. A. Bershad, B. Abolfathi, F. D. Albareti, C. Allende Prieto, A. Almeida et al., *AJ* **154** (2017) 28.
11. R. Neveux, E. Burtin, A. de Mattia, A. Smith, A. J. Ross, J. Hou et al., *MNRAS* **499** (2020) 210.
12. J. Hou, A. G. Sánchez, A. J. Ross, A. Smith, R. Neveux, J. Bautista et al., *MNRAS* **500** (2021) 1201.
13. S. Alam, M. Ata, S. Bailey, F. Beutler, D. Bizyaev, J. A. Blazek et al., *MNRAS* **470** (2017) 2617.
14. S. Alam, M. Aubert, S. Avila, C. Balland, J. E. Bautista, M. A. Bershad et al., *PRD* **103** (2021) 083533.
15. J. E. Bautista, N. G. Busca, J. Guy, J. Rich, M. Blomqvist, H. du Mas des Bourboux et al., *A&A* **603** (2017) A12.
16. H. du Mas des Bourboux, J. Rich, A. Font-Ribera, V. de Sainte Agathe, J. Farr, T. Etourneau et al., ascl:2106.018 (eprint) (2021).
17. A. J. Cuesta, M. Vargas-Magaña, F. Beutler, A. S. Bolton, J. R. Brownstein, D. J. Eisenstein et al., *MNRAS* **457** (2016) 1770.
18. H. Gil-Marín, J. E. Bautista, R. Paviot, M. Vargas-Magaña, S. de la Torre, S. Fromenteau et al., *MNRAS* **498** (2020) 2492.
19. J. E. Bautista, R. Paviot, M. Vargas Magaña, S. de la Torre, S. Fromenteau, H. Gil-Marín et al., *MNRAS* **500** (2021) 736.
20. C. Alcock & B. Paczynski, *Nature* **281** (1979) 358.
21. N. Kaiser, *MNRAS* **227** (1987) 1.
22. T. Matsubara & Y. Suto, *ApJL* **470** (1996) L1.
23. A.J.S. Hamilton, *The Evolving Universe. Selected Topics on Large-Scale Structure and on the Properties of Galaxies*, Astrophysics and Space Science Library **231** (1998).
24. A. Font-Ribera, D. Kirkby, N. Busca, J. Miralda-Escudé, N. Ross, A. Slosar et al., *JCAP* **2014** (2014) 027.
25. D. J. Eisenstein, H.-J. Seo, E. Sirko, D. N. Spergel, *ApJ* **664** (2007) 675.
26. N. Padmanabhan, X. Xu, D. J. Eisenstein, R. Scalzo, A. J. Cuesta, K. T. Mehta, E. Kazin, *MNRAS* **427** (2012) 2132.
27. J. E. Bautista, M. Vargas-Magaña, K. S. Dawson, W. J. Percival, J. Brinkmann, J. Brownstein et al., *ApJ* **863** (2018) 110.
28. F. Melia & M. López-Corredoira, *IJMP-D* **26** (2017) 1750055-265.

29. F. Melia & A.S.H. Shevchuk, *Mon. Not. R. Astron. Soc.* **419** (2012) 2579.
30. F. Melia, *The Cosmic Spacetime*, Taylor & Francis, Oxford (2020).
31. A. G. Riess, S. Casertano, W. Yuan, L. M. Macri & D. Scolnic, *ApJ* **876** (2019) 85.
32. H. Akaike, *IEEE Transactions on Automatic Control* **19** (1974) 716.
33. A. R. Liddle, *MNRAS* **377** (2007) L74.
34. K. P. Burnham & D. R. Anderson, *Model Selection and Multimodel Inference*, Springer, Heidelberg (2002).
35. F. Melia & R. S. Maier, *MNRAS* **432** (2013) 2669.
36. J. E. Cavanaugh, *Aust N Z J Stat* **46** (2004) 257.
37. G. Schwarz, *Annals of Statistics* **6** (1978) 461.
38. T. Delubac, J. E. Bautista, N. G. Busca, J. Rich, D. Kirkby, S. Bailey et al., *A&A* **574** (2015) A59.
39. F. Melia, *MNRAS* **481** (2018) 4855.
40. F. Melia, *A&A* **553** (2013) A76.
41. J. Liu & F. Melia, *PRSA* **476** (2020) 20200364.

## Appendix

We may gauge the validity of the approximate form of  $\chi^2$  in Equation (13) by comparing its outcome to that of a more detailed approach taking the covariance matrix,  $\mathbb{C}$ , into account. As noted earlier, the covariance matrix for  $d_{\text{com}}$  and  $d_{\text{H}}$  in the binnings at  $z = 0.38$  and  $0.51$  is available online.<sup>b</sup> In this case, we would write

$$\chi^2 = \mathbb{A}^T \mathbb{C}^{-1} \mathbb{A} , \quad (21)$$

where

$$\mathbb{A} \equiv \begin{pmatrix} |y_{\text{th}}(z_1) - y(z_1)| \\ \dots \\ |y_{\text{th}}(z_{N_b}) - y(z_{N_b})| \end{pmatrix} , \quad (22)$$

with  $N_b$  the number of bins (with some correlation between adjacent pairs only), and

$$\mathbb{C}_{ij} \equiv \langle [y_{\text{th}}(z_i) - y(z_i)] [y_{\text{th}}(z_j) - y(z_j)] \rangle \quad (23)$$

$$= \frac{1}{N_{ij} - 1} \sum_{k=1}^{N_{c,ij}} [y_{\text{th}}(z_k) - y(z_k)]^2 , \quad (24)$$

where  $N_{ij}$  is the total number of galaxies in bins  $i$  and  $j$ , and  $N_{c,ij}$  is the corresponding number of galaxies common to these two bins. Thus,

$$\mathbb{C}_{ij} = \sigma_i \sigma_j \frac{N_{c,ij}}{N_{ij} - 1} . \quad (25)$$

**Table 5.** Model comparison based solely on the AP effect (i) using Equation (21), including the covariance matrix; (ii) optimized parameters (if any); (iii) AIC; and (iv) KIC.

<sup>b</sup><https://svn.sdss.org/public/data/eboss/DR16cosmo/tags/v1-0-1/likelihoods/BAO-only/>

Model	$\chi_{\text{dof}}^2$	Parameter	AIC	KIC
$\Lambda$ CDM	2.18	$\Omega_{\text{m}} = 0.276 \pm 0.041$	8.53	9.53
<i>Planck</i> - $\Lambda$ CDM	1.98	–	7.92	7.92
$R_{\text{h}} = ct$	1.43	–	5.70	5.70

**Table 6.** Head-to-head model comparisons based solely on the AP effect, using the AIC and KIC values in Table 5.

Model Comparison	$\Delta$ AIC	AIC	$\Delta$ KIC	KIC
<i>Planck</i> - $\Lambda$ CDM vs. $R_{\text{h}} = ct$	2.22	25% vs. 75%	2.22	25% vs. 75%
$\Lambda$ CDM vs. $R_{\text{h}} = ct$	2.83	20% vs. 80%	3.83	13% vs. 87%

We define the relative number of common galaxies within the overlapping bins to be proportional to  $g_{ij}$ . Therefore,

$$\mathbb{C}_{ij} = \sigma_i \sigma_j g_{ij} . \quad (26)$$

From Equations (21), (22) and (26), one may therefore write

$$\begin{aligned} \chi^2 = \sum_{i=1}^{N_b-1} k_i (1 - g_{i,i+1}^2) & \left( \frac{[y_{\text{th}}(z_i) - y(z_i)]^2}{\sigma_i^2} + \right. \\ & \left. \frac{[y_{\text{th}}(z_{i+1}) - y(z_{i+1})]^2}{\sigma_{i+1}^2} - \right. \\ & \left. 2g_{i,i+1} \frac{|y_{\text{th}}(z_i) - y(z_i)|}{\sigma_i} \frac{|y_{\text{th}}(z_{i+1}) - y(z_{i+1})|}{\sigma_{i+1}} \right) . \end{aligned} \quad (27)$$

In this expression,  $k_i = 1$  for  $i = 1$  and  $N_b - 1$ , while  $k_i = 1/2$  for all the others. For the analysis in this paper (see Table 1), we also have  $N_b = 5$  and, taking  $g_{12} = C_{12}/\sqrt{C_{11} \times C_{22}}$  from the published covariance tables for the DR12 BAO-only,<sup>c</sup> for either  $d_{\text{com}}$  or  $d_{\text{H}}$  (which will also be the same for  $y(z)$  because, as shown by Eq. 25,  $g_{12}$  for any variable need only include the number of galaxies that are common in the two bins), we also have

$$\begin{aligned} g_{12} &= 0.42 \\ g_{23} &= 0 \\ g_{34} &= 0 \\ g_{45} &= 0 . \end{aligned} \quad (28)$$

<sup>c</sup><https://svn.sdss.org/public/data/eboss/DR16cosmo/tags/v1-0-0/likelihoods/BAO-only/>



The first three values reflect the overlap in redshift of the BOSS and e-BOSS bins of galaxies, while the last two values are zero because we neglect the correlations of galaxies with QSOs and of QSOs with the Ly- $\alpha$  forest.

If we repeat the calculations in § 2.1, though now using Equation (21) instead of Equation (13), we find the outcomes and likelihoods summarized in Tables 5 and 6. The numbers change slightly, but the relative likelihoods essentially remain intact. Most importantly, the prioritization of models based on the Alcock-Paczyński effect in the BAO measurements shows that  $R_{\text{h}} = ct$  is favored over both *Planck*  $\Lambda$ CDM and a more generic version of the standard model with  $\Omega_{\text{m}}$  as a free parameter.